3D Monte Carlo Device Simulation of NanoWire MOSFETs including Quantum Mechanical and Strain Effects

Andrea Ghetti* and Denis Rideau†
*STMicroelectronics - FTM - Advanced R&D, Via Olivetti 2, 20041 Agrate Brianza, Italy
Email: andrea.ghetti@st.com
†STMicroelectronics, 850 rue J. Monnet, BP 16, F-38926 Crolles CEDEX, France

***Abstract*— In this paper we report on 3D Monte Carlo device simulation of silicon NanoWire MOSFETs including quantum mechanical and strain effects. The newly developed simulator solves self-consistently in 1D, 2D or 3D the Schrödinger Eq. for the quantum mechanical correction of the potential, while mechanical strain effects are accounted for by an appropriate change of the band structure. The simulation program has been then applied to the simulation of silicon NanoWire MOSFETs achieving a good agreement with experimental data, demonstrating the feasibility of 3D semi-classical Monte Carlo simulation with quantum mechanical correction for very advanced devices.**

I. Introduction

In order to sustain the relentless downscaling of MOSFET physical dimensions aimed to improve circuit performance and cost, the ITRS roadmap forecasts sub-10nm devices by the year 2015 [1]. It is still not clear whether conventional planar bulk MOSFETs will meet this requirement because of the severe short channel effects they suffer. For this reason non-conventional MOSFETs, such as FD-SOI, double-gate (DG), FinFET etc., are being extensively investigated. Among the possible alternatives, NanoWire MOSFETs (NW-MOS) are gaining increasing popularity due to their superior channel control. This is achieved by reducing the silicon channel to a thin wire surrounded as much as possible by the gate (see, for example, Fig. 1). It is clear that for this kind of devices, the real 3D geometry plays a fundamental role that must be properly accounted for.

In addition, for such small devices, quantum mechanical (QM) effects, and notably charge confinement, greatly affect electrical characteristics. A boost in the performance may come from ballistic transport, but it is still under debate when scattering would not limit transport anymore. Finally, strain engineering has become a must to further improve performance. All these phenomena must be accurately accounted for in order to investigate, design and optimize NW-MOS.

In the first part of this paper we present a new simulator that accurately describes advanced devices such as NW-MOS considering all the above mentioned phenomena. It is based on 3D semi-classical Monte Carlo (MC) simulation that is intrinsically suited to describe highly non-local effects and scattering, and allows a straight forward inclusion of mechanical strain through an appropriate change of the silicon band structure. QM effects are accounted for by a correction of the potential provided by the self-consistent solution of the Schrödinger equation.

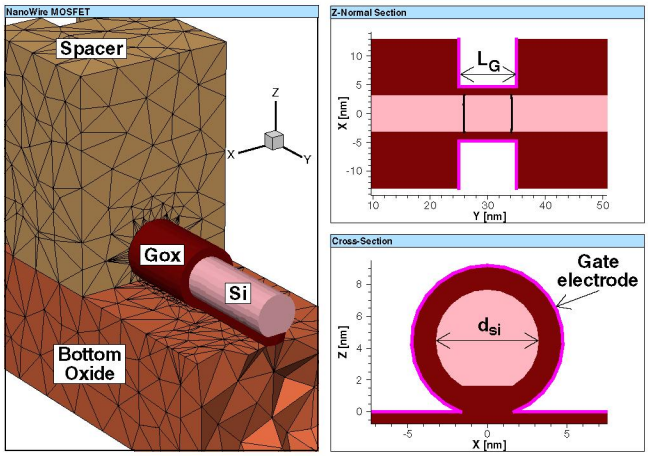

Fig. 1. Silicon NanoWire n-MOSFET experimentally characterized in [2] and simulated in this work. a) partial 3D view; b) horizontal (z-normal) section; c) channel cross-section. $L_G = 10$nm, $t_{ox} = 1.5$nm, $d_{si} = 6.5$nm. Not all dielectrics are shown.

In the second part of the paper, we show simulation results of silicon NanoWire MOSFETs provided by the new tool that achieve a good agreement with experimental data, demonstrating the feasibility of self-consistent Poisson-Schrödinger based 3D semi-classical Monte Carlo simulation for very advanced devices.

II. The New MC Simulator

Fig. 2 graphically depicts the interaction among the main blocks of the newly developed simulator (named MC++). It solves the Schrödinger Eq. (SE) and the Poisson Eq. (PE) self-consistently with the semi-classical 3D Monte Carlo simulation of carrier transport through an iterative procedure [3]. The linear PE is solved using standard box methods for the potential (Ψ) profile frequently enough (every 2fs) to assure time stability. The solution of the SE provides the QM correction term (Λ) of the potential accounting for charge quantization [3]. Both Ψ and Λ act as driving force in the Boltzmann Transport Eq. that is solved for via semi-classical

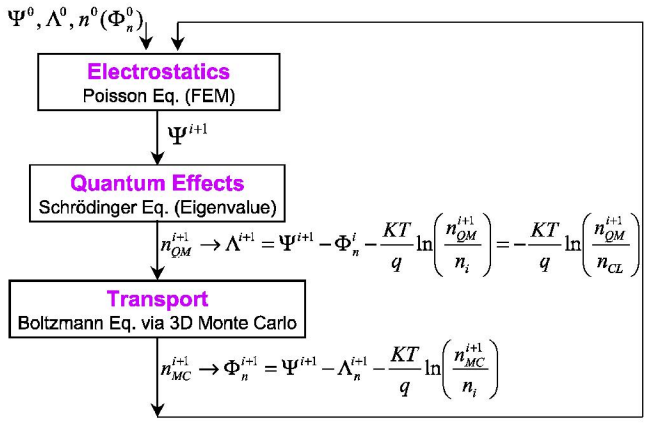

Fig. 2. Main blocks of the simulation program and their interactions. Simulation start by reading an initial guess computed with conventional programs.

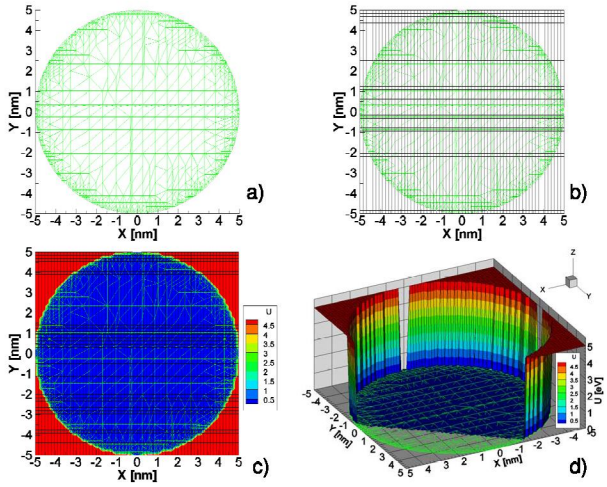

Fig. 3. Numerical solution of the 2D Schrödinger Eq. in the case of a circular well with R=5nm. a) initial finite element mesh; b) domain map to a uniform tensor product grid; c) contour plot of the energy profile; d) partial 3D view of the energy profile.

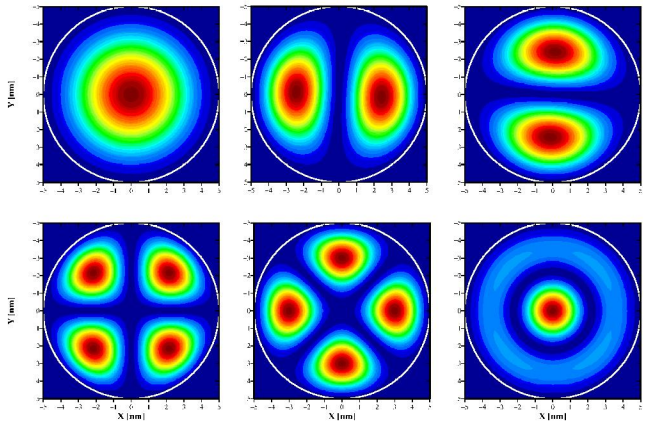

Fig. 4. Validation of the numerical solution of the 2D SE in the case of a circular well with R=5nm: squared wave function for the first 6 eigenstates.

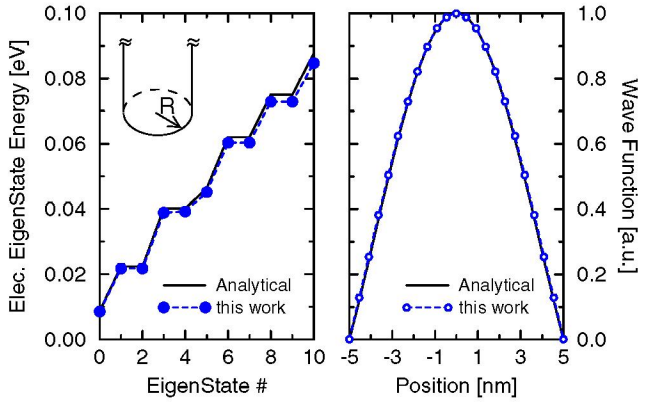

Fig. 5. Validation of the numerical solution of the 2D Schrödinger Eq. in the case of a circular well with R=5nm. Solid line: analytical solution; symbols: simulation. Left: eigenstate energy; right: first eigenstate wave function.

3D Monte Carlo simulation providing carrier/pseudo-potential profiles (n/Φ) to be used in the solution of both PE and SE.

In case of 3D structures, the SE is solved using a "Quasi 3D" approach [4]: the simulation domain is cut in several sections normal to the channel in which the 2D SE is solved for. Then, a continuous 3D description of the QM charge is recovered by interpolating the results of two adjacent sections. This approach is valid as long as the confinement region does not change shape, as in the case of NW-MOS [4]. The 2D SE is solved as in [5]. Assuming a rectangular domain with zero boundary conditions the solution can be expanded as $\Phi(x,y) = \sum_{ij}^{N} A_{ij} sin(k_x^i x) sin(k_y^j y)$. This allows to transform the 2D SE in a standard eigen-value problem (computed with highly optimized libraries [6]) involving the Fourier transform of Ψ, that can be efficiently computed exploiting FFT algorithms [7]. This methodology can be applied to *arbitrary* geometries, as illustrated in Fig. 3 for the case of a circular well. First, the initial domain (Fig. 3.a) is mapped onto a uniformly spaced tensor product grid (Fig. 3.b) needed by the FFT algorithm. Then, the energy profile is interpolated on the new grid. Points outside the initial domain are assigned an arbitrary high value (Fig. 3.c,d). This assures no wave penetration outside the original domain as shown in Fig. 4. The accuracy of this procedure is demonstrated in Fig. 5 comparing quantitatively the numerical and analytical solution for the same case of Figs. 3, 4.

Both physical and phase spaces are discretized with a tetrahedral mesh. This allows for the greatest flexibility in describing device geometry (see Fig. 1) and makes the free-flight equations linear [8], i.e. easy and fast to be solved. Fig. 6 shows two discretizations of the Brillouin Zone (BZ) used to describe the silicon anisotropic (full) band structure (BS). For bulk material (i.e. no strain) the irreducible wedge (IW, 1/48 of BZ) is enough (Fig. 6.a). Whereas, for a generic strain tensor, a larger portion of BZ must be used due to symmetry loss (for convenience we chose to store the entire BZ, see Fig. 6.b). Silicon band structure is computed with the Empirical Pseudo-potential Method [9] that accounts for strain-induced band structure distortion. The Density of State (DOS) is computed by directly calculating the area of the equi-energy surfaces, that are also stored in memory to speed up the determination of the state after scattering [8].

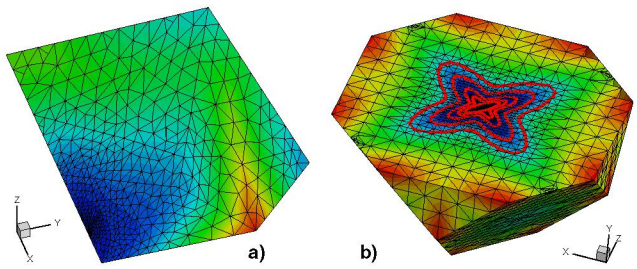

Fig. 6. Silicon band structure discretization: a) BZ irreducible wedge suitable for bulk material; b) full BZ (only half is shown) used for simulation with strain. Color contours refer to the energy of the lowest electron (a) and heavy hole sub-bands (b). Heavy hole sub-band has been computed under a 1GPa <110> uniaxial compressive stress that causes the distortion of the first contour level.

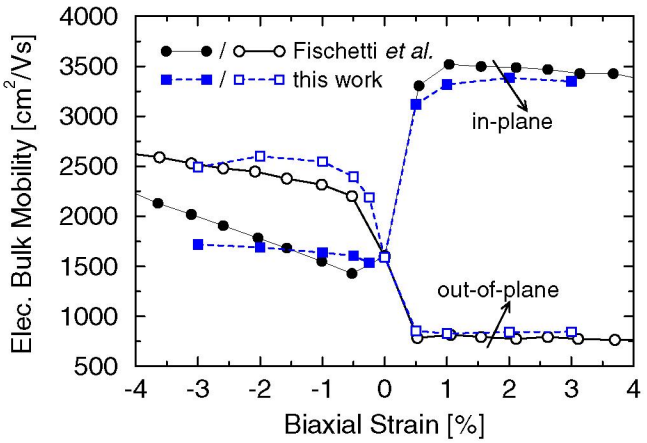

Fig. 7. Simulated electron bulk mobility (□/■) in comparison with calculation of [12] (○/●) for undoped silicon under biaxial strain. Closed/open symbols refer to in-plane/out-of-plane mobility.

Scattering mechanisms are assumed to be isotropic and to depend on strain through the variation of the DOS. Scattering mechanisms include: elastic acoustic phonon scattering, inelastic optical phonon scattering, ionized impurity scattering (isotropic model of [10]), impact ionization. Scattering against an interface is treated empirically as a mixture of reflecting and randomizing scattering [10]. Phonon scattering for electrons and holes has been extensively calibrated to reproduce a large variety of experiments including strain dependent mobility (Fig. 7 and [9], [11]).

III. NanoWire 3D MC Simulation

Using MC++ we simulated the NW-MOS reported in [2] and shown in Fig. 1. The actual iteration scheme is shown in Fig. 8. The simulation starts by reading an initial bias profile computed with conventional QM, i.e. density-gradient, hydrodynamic simulation (QM HD). Then, the Poisson and Schrödinger equations are solved self-consistently keeping constant the pseudo-potential found in the initial profile. This step has been introduced to provide a better initial guess for the potential QM correction (Λ^1 in Fig. 9) than the one provided by QM HD (Λ^0), thus speeding up convergence. Please notice

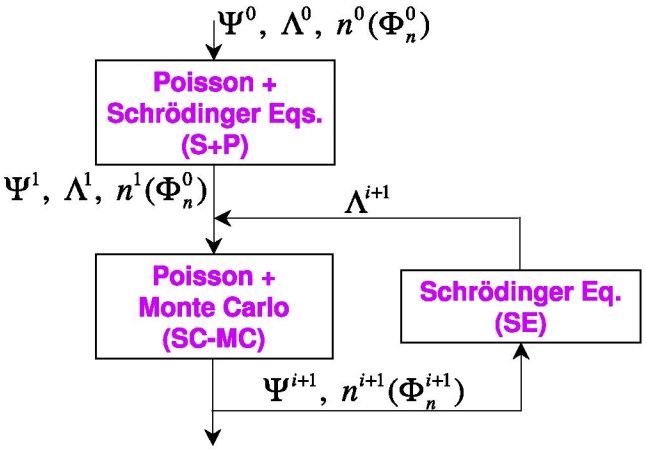

Fig. 8. Schematic representation of the iteration scheme. Convergence is reached after a few iterations.

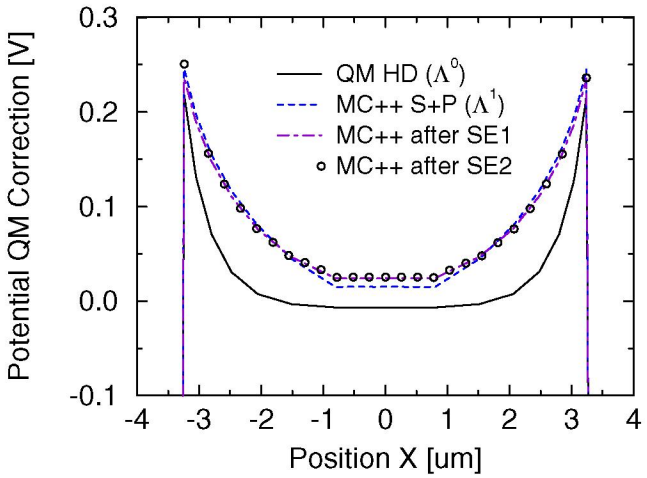

Fig. 9. Evolution of the potential QM correction during iterations. Λ^0 is the initial profile computed with conventional density-gradient hydrodynamic simulation (QM-HD). Λ^1 is the first guess provided by the self-consistent solution of the Schrödinger-Poisson Eq. (S+P).

in Fig. 9 that Λ^1 significantly deviates from Λ^0. Incidentally, this questions the accuracy of the standard density-gradient approach for 2D/3D cases. One note, indeed, that density-gradient is usually calibrated to reproduce Poisson-Schrödinger results in 1D. Next, the real iteration loop is entered by performing a Monte Carlo-Poisson self-consistent simulation until a steady-state solution is reached. This is necessary to get a smooth solution for the potential and carrier pseudo-potential to be used in the Schrödinger Eq. solution to update Λ. Notice that any "noise" on Ψ and Φ directly impacts Λ, and, if it is too large, may lead to unphysical results. The loop is then closed by solving the Schrödinger Eq. as explained in the previous section. As it is possible to see in Fig. 9, only a couple of iterations are needed to get a stable solution for Λ. Finally, once a stable solution for Λ has been obtained, a longer Monte Carlo-Poisson loop is performed to collect smoother statistics data.

All simulation results shown in the following have been obtained with the inclusion of strain. The strain tensor symmetry

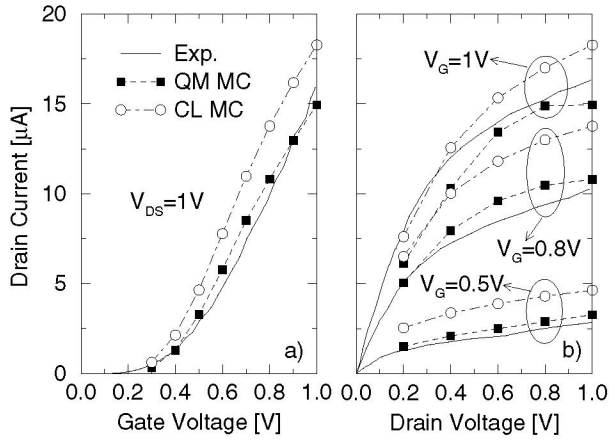

Fig. 10. Comparison of experimental (line) and simulated (symbols) drain current with (QM MC, ■) and without (CL MC, ○) QM correction. a) transcharacteristics; b) output characteristics.

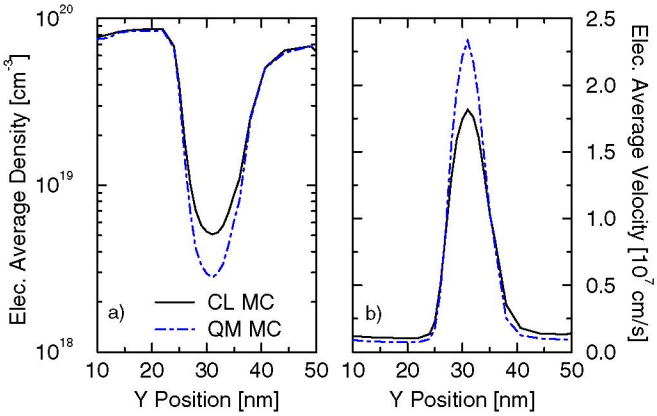

Fig. 11. Simulated electron density (a) and velocity (b) averaged on a channel cross-section as a function of the position for $V_G = 0.5V$, $V_{DS} = 1V$ with (QM MC, dot-dashed line) and without (CL MC, solid line) QM correction.

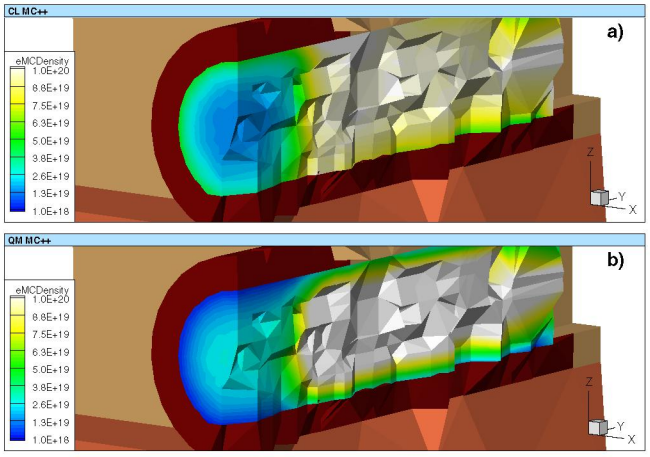

Fig. 12. Comparison of the electron concentration provided by CL (a) and QM (b) MC simulation for $V_G = 0.8V$, $V_{DS} = 0.2V$. Only 1/4 of the device is shown (drain end of the channel).

that can be inferred from the geometry of the device under investigation exhibits a biaxial compressive component in the plane perpendicular to the channel direction due to the gate all-around. Consequently, the current flows in the out-of-plane direction benefiting from the effect of the mechanical strain (Fig. 7). Using the analytical model of [13] and the process informations available in [2], the biaxial compressive strain is estimated to be 0.5%.

Simulated drain current with (QM MC) and without (CL MC) QM correction is compared to experimental data in Fig. 10. A good agreement with experimental data is found only if QM effects are accounted for, while CL MC provides an higher current, as expected (Fig. 10). This can be understood by looking at the electron concentration along the channel shown in Fig. 11.a. When QM effect are accounted for there is a decrease of the free carrier density inside the channel, thus a smaller current, simply because quantization reduces the number of allowed states. This effect is of particular importance for small devices such as NW-MOS. However, this is not the only effect due to quantization. Fig. 11.b also reports the average velocity along the channel in the two cases. When QM effects are accounted for, electrons attain a larger average velocity while transiting in the channel (≈+25%), thus partially compensating the reduced charge concentration (≈-50%). This is due to the particular shape of the carrier space distribution resulting from the inclusion of QM correction. As shown in Fig. 12.b, QM effects push electrons away from the interface providing the maximum concentration at the center of the NanoWire. On the contrary, without QM correction the maximum carrier concentration is attained at the gate oxide interface (Fig. 12.a). Thus, in this latter case, electrons will experience more surface scattering (as confirmed by the larger average number of surface scattering per simulated particle), resulting in a smaller velocity.

IV. Conclusion

In summary, we have presented a self-consistent Poisson-Schrödinger based 3D MC simulator also accounting for strain-induced effects. It has been exploited to simulate NW-MOS providing good agreement with experimental data. Therefore this tool represents a reasonable trade-off between accuracy, flexibility and usability, and can be used to investigate and design nanoscale devices.

References

[1] `http://public.itrs.net`.
[2] F.-L. Yang *et al.*, in *Proc. VLSI Technology Symposium*, p. 196, 2004.
[3] G. Kathawala *et al.*, in *IEDM Technical Digest*, 2003.
[4] J. Wang *et al.*, *Journal of Applied Physics*, vol. 96, no. 4, p. 2192, 2004.
[5] A. Abramo *et al.*, *IEEE Trans. on Electron Devices*, vol. 47, no. 10, p. 1858, 2000.
[6] E. Anderson *et al.*, *LAPACK Users' Guide*. Philadelphia, PA: Society for Industrial and Applied Mathematics, third ed., 1999.
[7] M. Frigo *et al.*, *Proceedings of the IEEE*, vol. 93, no. 2, p. 216, 2005.
[8] J. Bude *et al.*, *Semicond.Sci.Technol.*, vol. 9, p. 840, 1994.
[9] M. Feraille *et al.*, in *Proc. SISPAD Conference*, 2006.
[10] F. Bufler *et al.*, *IEEE Trans. on Electron Devices*, vol. 47, no. 10, p. 1891, 2000.
[11] P. Fantini *et al.*, in *IEDM Technical Digest*, p. 1013, 2005.
[12] M. Fischetti *et al.*, *Journal of Applied Physics*, vol. 80, no. 4, p. 2234, 1996.
[13] D.-B. Kao *et al.*, *IEEE Trans. on Electron Devices*, vol. 35, no. 1, p. 25, 1988.